



Carbon-Halogen Bond Activation with Powerful Heavy Alkaline Earth Metal Hydrides

Michael Wiesinger,^[a] Bastian Rösch,^[a] Christian Knüpfer,^[a] Jonathan Mai,^[a] Jens Langer,^[a] and Sjoerd Harder^{*[a]}

Reaction of $[(\text{DIPePBDI})\text{SrH}]_2$ with $\text{C}_6\text{H}_5\text{X}$ ($\text{X}=\text{Cl}, \text{Br}, \text{I}$) led to hydride-halogenide exchange ($(\text{DIPePBDI})=\text{HC}[(\text{Me})\text{CN}-2,6-(3\text{-pentyl})\text{phenyl}]_2$). Conversion rates increase with increasing halogen size ($\text{F}<\text{Cl}<\text{Br}<\text{I}$). Reaction of $[(\text{DIPePBDI})\text{SrH}]_2$ with $\text{C}_6\text{H}_5\text{F}$ was slow and ill-defined but addition of $\text{C}_6\text{H}_4\text{F}_2$ gave smooth hydride-fluoride exchange. After addition of THF the full range of Sr halogenides was structurally characterized: $[(\text{DIPePBDI})\text{SrX}\cdot\text{THF}]_2$ ($\text{X}=\text{F}, \text{Cl}, \text{Br}, \text{I}$). Mixtures of AeN''_2 and PhSiH_3 *in situ* formed less defined but more robust Ae metal hydride clusters ($\text{Ae}_x\text{N}''_y\text{H}_z$, $\text{Ae}=\text{Ca}, \text{Sr}, \text{Ba}$ and $\text{N}''=\text{N}(\text{SiMe}_3)_2$) which are able to hydrodefluorinate $\text{C}_6\text{H}_5\text{F}$. Conversion rates increase with increasing metal size ($\text{Ca}<\text{Sr}<\text{Ba}$). Also alkylfluorides (1-F-hexane, F-cyclohexane, 1-F-adamantane) could be converted

but, due to solubility problems of the Ba species, the fastest conversion was found for Sr. These $\text{AeN}''_2/\text{PhSiH}_3$ mixtures also converted SF_6 at room temperature to give undefined decomposition products. Addition of Me_6Tren to a $\text{SrN}''_2/\text{PhSiH}_3$ led to crystallization of $[\text{Sr}_6\text{N}''_2\text{H}_9\cdot(\text{Me}_6\text{Tren})_3]^+[\text{SrN}''_3]^-$; $\text{Me}_6\text{Tren}=\text{tris}[2\text{-(dimethylamino)ethyl}]\text{amine}$. After hydrodefluorination, $\text{Sr}_6\text{N}''_4\text{F}_8\cdot(\text{Me}_6\text{Tren})_2$ was formed and structurally characterized. Dissolution in THF led to cluster growth and the larger cluster $\text{Sr}_{16}\text{N}''_8\text{F}_{24}\cdot(\text{THF})_{12}$ is structurally characterized. DFT calculations support that hydrodehalogenation of halobenzenes follows a concerted nucleophilic aromatic substitution mechanism ($\text{cS}_\text{N}\text{Ar}$).

Introduction

Halogenated hydrocarbons are widely used as solvents and raw materials for pesticides, polymers, fire retardants, refrigerants and surfactants. While being highly useful in their intended purpose, halogenated materials may pose an environmental hazard due to accumulation within the food chain or cause ozone-depleting effects in the stratosphere.^[1–5] Therefore, the development of sustainable degradation methods to safely dispose such substances is of industrial and academic interest. Compared to C–X bonds with the heavier halogens, the activation of the C–F bond is particularly challenging. Bond dissociation energies rapidly increase along the series ($\text{kcal}\cdot\text{mol}^{-1}$): $\text{H}_3\text{C}-\text{I}$ 58 < $\text{H}_3\text{C}-\text{Br}$ 72 < $\text{H}_3\text{C}-\text{Cl}$ 84 < $\text{H}_3\text{C}-\text{F}$ 115).^[6] Several heterogeneous and homogeneous catalysts have been established for hydrodehalogenation, including Pt black, Raney metal alloys, transition metal salts and complexes of Pd, Pt, Ti, Ru, Ni and Rh.^[1,7] While these all involve transition metals, examples of defined main group metal complexes capable to

activate the C–F bond are scarce and, in some cases, are assisted by a transition metal. Generally these involve highly reactive low-valent main group metal species like $\text{Al}^{\text{I}[\text{B}–10]}$ and $\text{Mg}^{\text{I}[\text{I}1–14]}$ complexes that are capable to undergo oxidative addition to the C–F bond.

The C–F bond in fluorobenzene ($126\text{ kcal}\cdot\text{mol}^{-1}$) is arguably one of the strongest single bonds that carbon can form.^[15] Dimeric Mg^{I} complexes of the form $(\text{BDI})\text{MgMg}(\text{BDI})$ can only cleave activated C–F bonds in polyfluorinated aromatics with electron-poor π -systems ($\text{BDI}=\beta$ -diketiminato ligand; Scheme 1a). At least four F-substituents in the ring are needed and the presence of an *ortho*-F atom lowers the energy barrier for the transition state.^[11,12] Low-valent $(\text{BDI})\text{Al}^{\text{I}}$ complexes can cleave the C–F bond in a ring with at least three F-substituents (Scheme 1b), requiring long reaction times and high temperatures, however, addition of catalytic quantities of $\text{Pd}(\text{PCy}_3)_2$ also allowed conversion of $\text{C}_6\text{H}_4\text{F}_2$ and $\text{C}_6\text{H}_5\text{F}$ under mild conditions.^[16–18] The mildest conditions (-30°C) for C–F bond cleavage in $\text{C}_6\text{H}_5\text{F}$ have been reported for a heterobimetallic $\text{Al}^{\text{I}}\text{-Rh}^{\text{I}}$ complex.^[19]

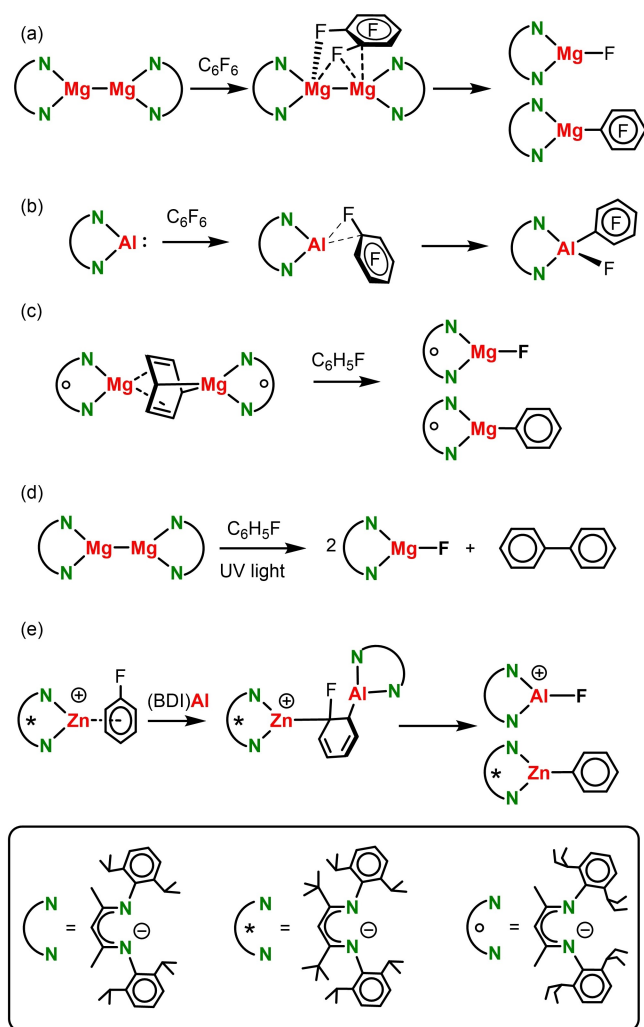
We reported C–F bond cleavage in fluorobenzene using a Mg complex with a strongly reducing, anti-aromatic $\text{C}_6\text{H}_6^{2-}$ anion, but conditions were harsh (5 days, 100°C); Scheme 1c.^[14] A mild, room temperature protocol was recently presented relying on a photoactivated $(\text{DIPPPBDI})\text{MgMg}(\text{DIPPPBDI})$ complex inducing a radical process with fluorobenzene to yield $[(\text{DIPPPBDI})\text{MgF}]_2$ and biphenyl (Scheme 1d); $(\text{DIPPPBDI})=\text{HC}[(\text{Me})\text{CN}-2,6\text{-(isopropyl)phenyl}]_2$.^[20] Most recently, we reported that the combination of $(\text{BDI})\text{Al}^{\text{I}}$ and a “naked” cationic β -diketiminato Zn complex cleaves the C–F bond in $\text{C}_6\text{H}_5\text{F}$ instantly at 20°C following an unusual dearomatization/aromatization mechanism (Scheme 1e).^[21] This heterobimetallic system also allowed

[a] M. Wiesinger, B. Rösch, C. Knüpfer, J. Mai, Dr. J. Langer, Prof. Dr. S. Harder
Inorganic and Organometallic Chemistry,
Universität Erlangen-Nürnberg,
Egerlandstraße 1, 91058, Erlangen, Germany
E-mail: sjoerd.harder@fau.de
<https://www.harder-research.com>

Supporting information for this article is available on the WWW under
<https://doi.org/10.1002/ejic.202100529>

Part of a joint Special Collection on “Main Group Catalysis”. Please click here
for more articles in the collection.

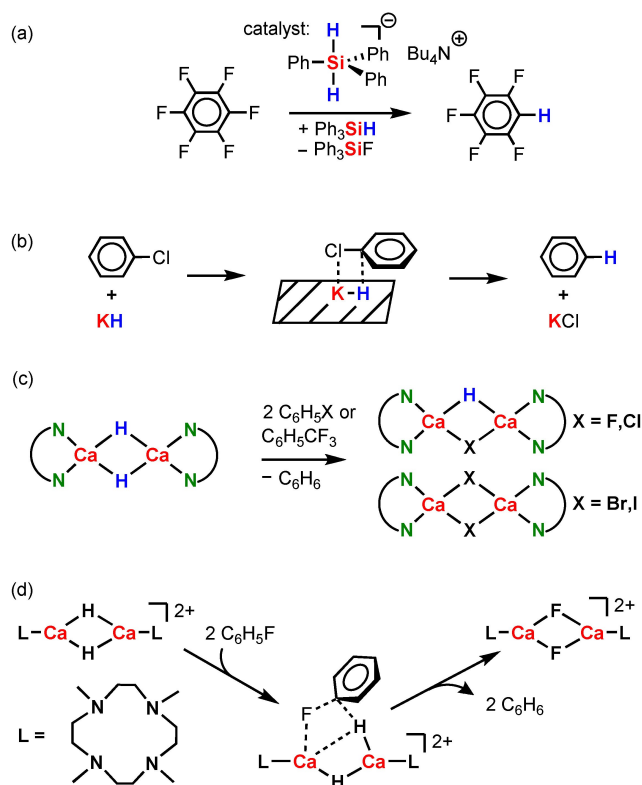
© 2021 The Authors. European Journal of Inorganic Chemistry published by
Wiley-VCH GmbH. This is an open access article under the terms of the
Creative Commons Attribution License, which permits use, distribution and
reproduction in any medium, provided the original work is properly cited.



Scheme 1. Activation of C–F bonds using low-valent main group metal complexes.

immediate scission of the even more electron-rich *p*-fluorotoluene.

Alternatively, hydrodehalogenation goes via nucleophilic aromatic substitution (S_NAr) with nucleophilic metal hydride reagents. Combinations of nano-sized NaH and $LiAlH_4$ with transition metal or lanthanide salts were found highly potent reagents for converting monofluoroarenes to arenes.^[22–24] Relying exclusively on main group (semi)metals, few systems have been identified that allow direct substitution of the C–X bond. Ogoshi and coworkers reported the silicate mediated hydrodefluorination of fluoroarenes with silanes and although this reaction is catalytic, it only works for polyfluorinated arenes (Scheme 2a).^[25] At an early stage the Pierre group demonstrated that KH converts C_6H_5X into benzene but this method only worked for $X = Cl, Br$ and I (for C_6H_5F ca. 5% conversion was found).^[26] The reaction was proposed to follow a concerted nucleophilic aromatic substitution mechanism (cS_NAr , Scheme 2b) but depending on solvent also a single-electron-transfer mechanism is possible.^[27] The commonly used drying agent CaH_2 was identified to be capable of complete hydrodechlori-



Scheme 2. Activation of C–F bonds using main group (semi)metal hydrides.

nation of C_6Cl_6 and C_6H_5Cl to benzene and $CaCl_2$ in a mechanochemical approach.^[28] While authors believe this technology could be transferred to fluorinated substrates, evidence is currently not reported. Since the low solubility of CaH_2 limits its reactivity, hydrocarbon-soluble Ca hydride complexes would be highly advantageous. In solution, the first defined Ca hydride complex $[(DIPPBDI)CaH \cdot THF]_2$ has shown astonishing reactivities.^[29,30]

The THF-free analogue $[(DIPPBDI)CaH]_2$ was found to be even more reactive.^[31] The Hill and Maron groups demonstrated that it is able to substitute the halogen in C_6H_5X ($X = Cl, Br, I$) giving benzene and $[(DIPPBDI)CaX]_2$ or $(DIPPBDI)CaH/(DIPPBDI)CaX$ complexes (Scheme 2c), however, the reaction with C_6H_5F led to ill-defined products.^[32] The Okuda and Maron groups recently reported a dicationic dimeric Ca hydride complex that also cleaved the C–F bond in unactivated C_6H_5F but full F–H substitution needed two days at 60 °C (Scheme 2d).^[33] These reactions are proposed to follow the mechanism for nucleophilic aromatic substitution in which the cation Ca^{2+} has recently been shown to play a unique role. Being a large, soft cation it prefers bonding to the arene π -system, activating the ring for substituent exchange.^[31,34] The larger cations Sr^{2+} and Ba^{2+} are even much more efficient in activating arenes for nucleophilic aromatic substitution. We recently introduced the first Ae metal catalysts for Hydrogen-Isotope-Exchange in arenes and reported a catalytic scenario for benzene deuteration by D_2 .^[35,36] The catalysts can either be well-defined complexes (e.g. $[(BDI)SrH]_2$)^[35] or ill-defined *in situ* generated

HAeN(SiR₃)₂ aggregates (Ae = Ca, Sr, Ba);^[36] examples of such mixed Ae metal hydride-amide aggregates have been characterized.^[37,38] The latter are also highly active catalysts in the hydrogenation of alkenes and the more challenging arenes, also following a nucleophilic aromatic substitution mechanism.^[39] In addition, while Hill reported stoichiometric benzene alkylation with [(^{DIPeP}BDI)Ca(alkyl)]₂,^[31] we published the first example for catalytic benzene alkylation with the heavier Sr hydride dimer following the steps: [(BDI)SrH]₂ + 2 H₂C=CH₂ → [(BDI)SrEt]₂ and [(BDI)SrEt]₂ + C₆H₆ → [(BDI)SrH]₂ + C₆H₅Et, a reaction which is competing with ethylene polymerization and the formation of higher alkylbenzenes.^[35] We now report initial studies on C–X bond activation in non-activated C₆H₅X substrates (X = F, Cl, Br, I) with heavier Ae metal hydrides.

Results and Discussion

Hydrodehalogenation with defined Ae metal hydride complexes

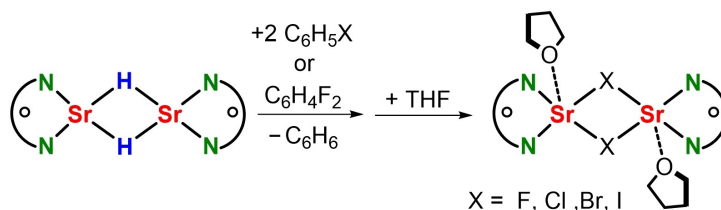
Since solvent-effects in heteroleptic β-diketiminato Ca hydride complexes can play an important role,^[40] we investigated hydrodehalogenation with the THF adduct [(^{DIPeP}BDI)CaH·THF]₂. Like the THF-free complex, [(^{DIPeP}BDI)CaH·THF]₂ reacted instantaneously with iodobenzene at room temperature to give benzene and [(^{DIPeP}BDI)CaI·THF]₂ (Figure S30). Minor quantities of the homoleptic complex (^{DIPeP}BDI)₂Ca have been detected with full conversion to homoleptic complexes at 60 °C. With fluorobenzene no reaction was observed but heating 42 h at 60 °C gave full conversion of the Ca hydride complex. Larger quantities of literature-known [(^{DIPeP}BDI)CaF·THF]₂^[41] could be detected by ¹H and ¹⁹F NMR (Figure S31–32) but the reaction is not clean. These experimental observations demonstrate that nucleophilic substitution of halides in halobenzenes are also possible with the THF adduct [(^{DIPeP}BDI)CaH·THF]₂. Much higher reactivities are expected for the heavier Sr hydride complexes.

We recently introduced a superbulky β-diketiminato ligand, abbreviated as ^{DIPeP}BDI (Scheme 3), that is able to control detrimental Schlenk equilibria for heteroleptic complexes of Ca, Sr and Ba (^{DIPeP}BDI = HC[(Me)CN-2,6-(3-pentyl)phenyl]₂).^[42] This very bulky ligand enabled synthesis of the Sr hydride complex [(^{DIPeP}BDI)SrH]₂ that is also in aromatic solvents stable towards ligand exchange until at least 70 °C.^[35] Dissolution of complex [(^{DIPeP}BDI)SrH]₂ in halobenzene C₆H₅X (X = I, Br, Cl) led in all cases to hydride-halide exchange. With increasing size of X, the

reaction conditions steadily become less harsh: C₆H₅Cl (60 °C, 12 h), C₆H₅Br (20 °C, 14 h), C₆H₅I (20 °C, < 1 h). After removal of excess halobenzene and crystallization from a hexane-THF mixture the dimeric Sr halide complexes [(^{DIPeP}BDI)SrX·THF]₂ could be isolated as colorless crystals in yields of 53 % (X = Cl), 72 % (X = Br) or 43 % (X = I); Scheme 3. Twofold H–X exchange could also be achieved in benzene solutions containing only two equivalent of C₆H₅X per Sr hydride dimer but is clearly slower. In contrast to observations by Hill on the reactivity of Ca hydrides, in none of the case could we isolate the intermediate single exchange product, *i.e.* the mixed halide-hydride dimer. This is due to the much higher reactivity of Sr hydrides compared to Ca hydrides but also may be related to the solubilizing effect of the ^{DIPeP}BDI substituents which prevent crystallization of poorly soluble mixed halide-hydride intermediates. Reaction of [(^{DIPeP}BDI)SrH]₂ with C₆H₅F was found to be slower and needed more forcing conditions (60 °C, 3 days) which led to ill-defined products. However, reaction with 1,2-difluorobenzene, which is slightly activated to C–F bond cleavage, was found to be much faster (60 °C, 4 h) and, after work-up and recrystallization from hexane/THF, crystals of [(^{DIPeP}BDI)SrF·THF]₂ were isolated in 56 % yield.

Dissolved in toluene, all halide complexes proved to be stable towards ligand exchange reactions even under reflux conditions. Reaction with the silanes PhSiH₃, Et₃SiH, Ph₃SiH, or (EtO)₃SiH did not form the initial Sr hydride complex which disables a possible catalytic hydrodehalogenation scenario using silanes as a H-source.

All Ae metal halide complexes crystallize as centrosymmetric dimers of constitution [(^{DIPeP}BDI)SrX·THF]₂ (the fluoride complex is exemplary shown in Figure 1) but despite their similar architecture they do not crystallize isomorphous. Although each complex crystallizes in a different crystal lattice with a different packing, their structures compare well to each other. In all cases, the halide anions bridge the two strontium metal atoms in μ₂-fashion. The coordination sphere of each Sr metal was further saturated by an *N,N*-chelating ^{DIPeP}BDI ligand and a THF ligand [Sr–O: 2.493(2)–2.594(2) Å], giving the Sr metal centers a coordination number of five. In all cases metal coordination is completed by anagostic Sr...CH₃CH₂ interactions which range from Sr...C = 3.302 Å to 3.413 Å. While Sr–N [2.492(2)–2.553(3) Å] and Sr–O [2.493(2)–2.594(2) Å] bond distances are in a narrow range, the Sr–X bond lengths increase with halogen size. They are, however, closely comparable to Sr–X bonds in similar [(^{DIPeP}BDI)SrX]₂·(THF)_n complexes (Table 1).^[43,44]



Scheme 3. Reaction of [(^{DIPeP}BDI)SrH]₂ with C₆H₅X (X = I, Br, Cl) or C₆H₄F₂.

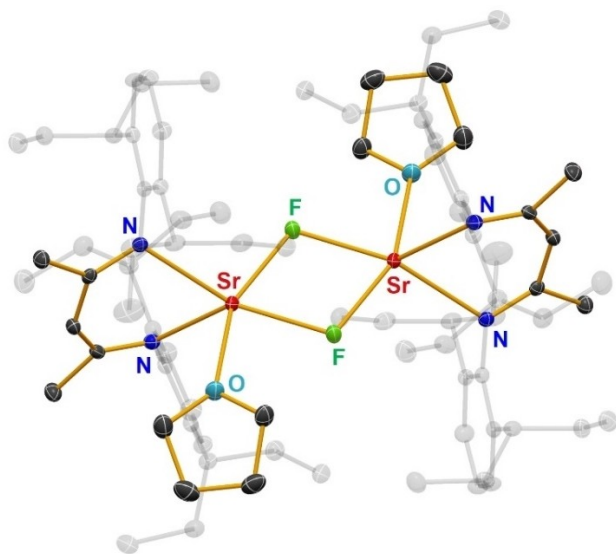


Figure 1. Solid state structure of $[(\text{DIPePBDI})\text{SrF} \cdot (\text{THF})]_2$; H atoms not shown (50% probability).

Table 1. Comparison of the Sr–X distances in $[(\text{DIPePBDI})\text{SrX} \cdot \text{THF}]_2$ with values reported for $[(\text{DIPePBDI})\text{SrX}]_2 \cdot (\text{THF})_n$.^[43,44] Bold values represent mean averages.

	$[(\text{DIPePBDI})\text{SrX} \cdot \text{THF}]_2$	$[(\text{DIPePBDI})\text{SrX}]_2 \cdot (\text{THF})_n$
Sr–F	2.318(1)–2.376(1) 2.347	2.317(1)–2.333(1) ^[a] 2.325
Sr–Cl	2.825(2)–2.900(1) 2.860	2.821(1)–2.890 ^[a] 2.856
Sr–Br	2.9774(5)–3.1043(6) 3.0282	unknown
Sr–I	3.2054(7)–3.3272(7) 3.2649	3.2284(4)–3.3100(3) ^[b] 3.2567

[a] $n = 3$: One of the Sr metals is coordinated with one THF ligand while the other is bound to two THF ligands. The listed bond distances are those for the metal atom with a comparable coordination number of five. [b] $n = 2$.

Attempts to extend the scope of fluorinated substrates to fluoroalkanes like 1-fluorohexane, fluoro-cyclohexane or 1-fluoroadamantane were not successful. Contrary to expectations, $[(\text{DIPePBDI})\text{SrH}]_2$ reacted only sparingly with these substrates, even at elevated temperatures just below its decomposition temperature of 70 °C.^[35] This may be due to considerable steric shielding of the reaction center by the bulky DIPePBDI ligands. We were therefore interested in more open and robust Ae metal hydride systems which are also at higher temperatures stable.

Hydrodefluorination with undefined Ae metal hydride complexes

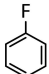
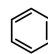
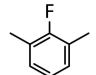
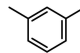
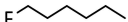
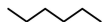
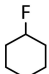
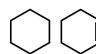
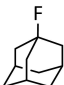

It has been shown that the sterically moderately encumbered Ae metal *bis*-amide complexes $\text{Ae}[\text{N}(\text{SiMe}_3)_2]_2$, abbreviated as AeN''_2 (Ae = Ca, Sr, Ba), react *in situ* with H_2 or PhSiH_3 to large hydride clusters^[37,38] that are efficient catalysts for imine or

alkene hydrogenation^[45–47] or hydrosilylation.^[48] These studies also showed that, although these systems are less defined, they are highly robust and tolerate higher temperatures. Encouraged by the hydrodehalogenation capability of the well-defined strontium hydride complex $[(\text{DIPePBDI})\text{SrH}]_2$, we wondered whether simple amides could also be effective in the activation of the most challenging C–F bond.

The amides AeN''_2 (Ae = Ca, Sr, Ba) were reacted with two equivalents of $\text{C}_6\text{H}_5\text{F}$ and three equivalents of PhSiH_3 under forcing conditions (120 °C, 6–24 h, toluene- d_8) and conversion was monitored by ^1H NMR and GC-MS. The $\text{SrN}''_2/\text{PhSiH}_3$ combination gave after 6 h a fluorobenzene-to-benzene conversion of 54% (or 78% after 12 h); (Table 2, entries 1–2). The temperature could be lowered to 60 °C but this elongated the reaction time significantly (entry 3). The lighter CaN''_2 is clearly less reactive than SrN''_2 (entry 4) and not only gave F–H exchange but also F–N'' exchange was observed and traces of $\text{C}_6\text{H}_5\text{N}''$ were detected. The heavier BaN''_2 was found to be most reactive, reaching a conversion of up to 85% after 6 h (entries 5–6). Using the most active reagent BaN''_2 , the PhSiH_3 content was increased to 10 equivalents but this had clearly a detrimental effect (entry 6). This is attributed to the formation of insoluble $(\text{BaH}_2)_\infty$ or to formation of less reactive silanates like $\text{Ba}[\text{PhSiH}_2]_2$. The silanes $(\text{MeO})_3\text{SiH}$, $(\text{EtO})_3\text{SiH}$, Et_3SiH or Ph_3SiH were not effective. Using $\text{AeN}''_2/\text{PhSiH}_3$ combinations, we also were able to hydrodefluorinate most challenging substrates like 2,6-dimethyl-fluorobenzene with a sterically protected C–F bond and an electron-rich aryl ring (entries 7–9). While CaN''_2 failed, with BaN''_2 a conversion of 58% (12 h) could be reached.

Following success in the activation of aromatic C–F bonds, the $\text{AeN}''_2/\text{PhSiH}_3$ combinations were investigated in the hydrodefluorination of alkyl C–F bonds. 1-Fluorohexane was converted to hexane following the reactivity order $\text{Ca} < \text{Ba} < \text{Sr}$ (entries 10–12). Since Ba amides and hydrides are generally more reactive than their Sr congeners, this reactivity order is unexpected. It may partially be explained by the observation that in reactions with the $\text{BaN}''_2/\text{PhSiH}_3$ combination a considerable quantity of a precipitate was formed. The assumption that these are likely insoluble $\text{BaN}''\text{H}$ clusters was supported by the fact that a CD_3OD quench of the insoluble material led to vigorous gas evolution and detection of H–D and N''D by ^1H NMR. The formation of a precipitate is explained by the fact that alkylfluorides are poorer solvents than fluorobenzene. Also for 1-fluorohexane partial F–N'' exchange was observed with the $\text{CaN}''_2/\text{PhSiH}_3$ combination but using the heavier amides SrN''_2 and BaN''_2 the product 1-N''-hexane could not be detected. For the secondary alkylfluoride fluoro-cyclohexane (entries 13–15), hydrodefluorination with BaN''_2 is also slower than with SrN''_2 . In this case not only cyclohexane but also cyclohexene is formed. This side-reaction, which presumably follows a deprotonation-elimination pathway, strongly depends on metal size and becomes more important with decreasing metal size: $\text{Ba} < \text{Sr} < \text{Ca}$. Also for the tertiary 1-fluoro-adamantane SrN''_2 performed better than BaN''_2 (entries 16–17) and in this case no elimination side-products were observed. The

Table 2. Hydrodefluorination with $\text{AeN}''_2/\text{PhSiH}_3$ combinations in toluene- d_8 ; F-substrate concentration: 0.16–0.18 M (conversion determined by GC-MS).

Entry	AeN''_2	Substrate [2 eq]	PhSiH_3 [eq]	T [°C]	t [h]	Product(s)	Conv. [%]
1	SrN''_2		3	120	6		54
2	SrN''_2		3	120	12		78
3	SrN''_2		3	60	24		50
4	CaN''_2		3	120	6		11 ^[a]
5	BaN''_2		3	120	6		85
6	BaN''_2		10	120	12		21
7	CaN''_2		3	120	12		1
8	SrN''_2		3	120	12		51
9	BaN''_2		3	120	12		58
10	CaN''_2		3	120	12		61 ^[b]
11	SrN''_2		3	120	12		100
12	BaN''_2		3	120	12		82
13	CaN''_2		3	120	12		7/86 ^[c]
14	SrN''_2		3	120	12		28/65
15	BaN''_2		3	120	12		55/13
16	SrN''_2		3	120	12		73
17	BaN''_2		3	120	12		57

[a] Additional 6 % of $\text{N}''\text{C}_6\text{H}_5$ were identified by GC-MS. [b] Additional 39 % of $\text{N}''\text{C}_6\text{H}_{13}$ were identified by GC-MS. [c] Additional 7 % of $\text{N}''\text{C}_6\text{H}_{11}$ were identified by GC-MS.

general reactivity trend is that conversion slows down in the order: primary > secondary > tertiary fluoroalkanes.

The efficiency of $\text{AeN}''_2/\text{PhSiH}_3$ mixtures as a hydrodefluorination reagent was further investigated by reaction with SF_6 , a highly stable fluorine compound. Sulfur hexafluoride, which finds application as an insulator in high voltage electrical equipment, is one of the most potent greenhouse gases, surpassing CO_2 by a factor of 23.900.^[49] Chemical breakdown of SF_6 with LiAlH_4 at room temperature has been previously reported,^[50] but is extremely slow (4–7 days). Reaction of SF_6 with SrN''_2 or BaN''_2 in the presence of PhSiH_3 at room temperature is fast. Monitoring with ^{19}F -NMR showed a gradual decrease of the SF_6 signal at -58.3 ppm and complete disappearance within 1 h, but no new ^{19}F signal set was observed. This is explained by formation of considerable quantities of an insoluble yellow precipitate containing 1.77 w% S but also organic matter (C 24.14 w%, H 3.77 w%, N 1.64 w%). Its complete insolubility complicated any further analyses. We propose precipitation of larger metal clusters containing a variety of anions like N''^- , H^- , F^- but also SF_5^- or S^{2-} could be expected.^[51] Room temperature destruction of SF_6 by *in situ* formed Sr or Ba hydrides demonstrates the very high reactivity of the heavier Ae metal hydrides.

Although the $\text{AeN}''_2/\text{PhSiH}_3$ combination is an effective hydrodefluorination reagent, we have not been able to isolate well-defined Ae-fluoride complexes from reaction mixtures. Since the addition of PMDTA (pentamethyldiethylenetriamine) to $\text{AeN}''_2/\text{PhSiH}_3$ mixtures led to isolation of well-defined Ae metal hydride clusters of formula $\text{Ae}_6\text{N}''_3\text{H}_9 \cdot (\text{PMDTA})_3$ (Ae = Ca or Sr),^[37] we attempted to isolate defined Ae metal fluoride clusters by hydrodefluorination with $\text{AeN}''_2/\text{PhSiH}_3/\text{PMDTA}$

mixtures. As these experiments were unsuccessful, we replaced PMDTA by the tetradentate ligand Me_6Tren (*tris*[2-(dimethylamino)ethyl]amine).

Heating a $\text{SrN}''_2/\text{PhSiH}_3/\text{Me}_6\text{Tren}$ mixture alone led to crystallization of the salt $[\text{Sr}_6\text{N}''_2\text{H}_9 \cdot (\text{Me}_6\text{Tren})_3]^+[\text{SrN}''_3]^-$ which was characterized by X-ray diffraction (Figure 2a) but could not be obtained pure in larger quantities. Its crystal structure is strikingly similar to that of the previously reported $\text{Sr}_6\text{N}''_3\text{H}_9 \cdot (\text{PMDTA})_3$ cluster in which the core of the cluster consists of six Sr^{2+} cations at the corners of an octahedron, one interstitial $\mu_6\text{-H}^-$ and eight $\mu_3\text{-H}^-$ anions that cap the Sr_3 -faces of the octahedron. The cluster is further stabilized by two terminal N''^- ligands and three neutral, tetradentate Me_6Tren ligands. Its positive charge is balanced by the SrN''_3^- anion. The bond distances in the cation $\text{Sr}_6\text{N}''_2\text{H}_9 \cdot (\text{Me}_6\text{Tren})_3^+$ ($\text{Sr-H}_{\text{center}}$ avg. 2.70 Å; $\text{Sr-H}_{\text{outer}}$ avg. 2.47 Å) are close to identical with those in the neutral cluster $\text{Sr}_6\text{N}''_3\text{H}_9 \cdot (\text{PMDTA})_3$ ($\text{Sr-H}_{\text{center}}$ avg. 2.69 Å; $\text{Sr-H}_{\text{outer}}$ avg. 2.43 Å) (Table S2).

Heating $\text{SrN}''_2/\text{PhSiH}_3/\text{Me}_6\text{Tren}$ in a mixture of fluorobenzene and 1-fluorohexane led to immediate conversion of 1-fluorohexane, supporting the more facile hydrodefluorination of alkylfluorides vs. arylfluorides, and crystallization of centrosymmetric $\text{Sr}_6\text{N}''_4\text{F}_8 \cdot (\text{Me}_6\text{Tren})_2$. This complex could be isolated in crystalline purity (yield: 10%) and its crystal structure could be determined unequivocally (Figure 2b). The core of the cluster is formed by six Sr^{2+} cations in an octahedral arrangement with an average $\text{Sr} \cdots \text{Sr}$ distance of 3.9343 Å which is slightly larger than that in the Sr hydride cluster $\text{Sr}_6\text{N}''_2\text{H}_9 \cdot (\text{Me}_6\text{Tren})_3^+$ (3.8135 Å). Although there is no interstitial F^- anion, eight $\mu_3\text{-F}^-$ anions cap the Sr_3 -faces of the octahedron and span a cube (Figure 2c). The Sr_6H_9 -core can be regarded as a sub-unit of the

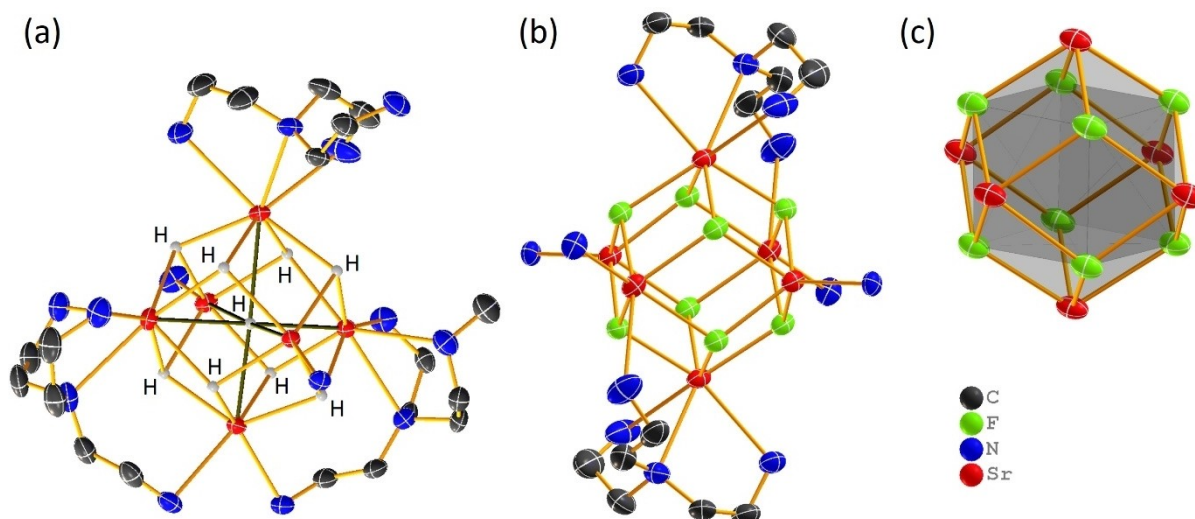


Figure 2. (a) Crystal structure of $[\text{Sr}_6\text{N}''_4\text{H}_9 \cdot (\text{Me}_6\text{Tren})_3]^+[\text{SrN}_3]^-$; methyl groups, SiMe_3 groups, and the anion SrN_3^- have been omitted for clarity. All hydride atoms have been identified in the difference Fourier map and were refined isotropically. (b) Crystal structure of $\text{Sr}_6\text{N}''_4\text{F}_8 \cdot (\text{Me}_6\text{Tren})_2$. Methyl groups and SiMe_3 groups have been omitted for clarity. (c) The $[\text{Sr}_6\text{F}_8]^{4+}$ core. Fluoride anions (green) describe a cube in an octahedron spanned by strontium cations (red). All ellipsoids are shown with 50% probability.

SrF_2 fluorite crystal lattice, *i.e.* a face-centered-cubic packing of Sr^{2+} cations with F^- in the eight tetrahedral holes (coordination numbers: $\text{Sr}=8$, $\text{F}=4$). The neutral cluster is stabilized by four terminal N'' ligands and two neutral, tetradentate Me_6Tren ligands which prevent further growth to $(\text{SrF}_2)_\infty$. The average $\text{Sr}-(\mu_3\text{-F})$ bond length of 2.434 Å compares well to that in $\text{Sr}_{10}\text{F}_8(2,4,6\text{-trimethylphenolate})_{12} \cdot (\text{dme})_4$ (dme = dimethoxyethane) cluster (avg. $\text{Sr}-\text{F}$ 2.44 Å), which to the best of our knowledge is the only other reported $\text{Sr}-\text{F}$ cluster to date.^[52]

The most striking difference between the two hexanuclear Sr hydride and fluoride clusters is found in their core structures. Compared to the hydride cluster with a $\text{Sr}_6\text{H}_9^{3+}$ core, the $\text{Sr}_6\text{F}_8^{4+}$ core lacks an interstitial $\mu_6\text{-F}^-$ anion. This may originate from size differences. Based on ionic bond radii in alkali metal salts (coordination number = 6) the fluoride ion radius of 1.547 Å is larger than that for the hydride estimated at 1.399 Å.^[53] However, argumentation with ionic radii should be taken with caution since effective ionic radii in the literature vary significantly.^[54–56] DFT calculations (B3PW91/def2tzvp) on a $\text{Sr}_6\text{F}_9^{3+}$ core indicated that an interstitial $\mu_6\text{-F}^-$ anion would fit. Calculating the energy of X^- anion capture in a $\text{Sr}_6\text{X}_8^{4+}$ cage showed that this process, which due to electrostatic attraction is highly exergonic, is even more exergonic for $\text{X}^- = \text{F}^-$ ($\Delta G = -485.3$ kcal/mol) than for $\text{X}^- = \text{H}^-$ ($\Delta G = -358.7$ kcal/mol) (Table S5). Atoms-In-Molecules (AIM) analysis showed for the hydride cluster unusual $\text{H}^- \cdots \text{H}^-$ bond paths between the interstitial hydride and the eight outer hydrides with electron densities in the bond-critical-points (*bcp*'s) of $0.094 \text{ e} \cdot \text{\AA}^{-3}$. For $\text{Sr}_6\text{F}_9^{3+}$ similar weakly bonding $\text{F}^- \cdots \text{F}^-$ interactions were found with electron densities in *bcp*'s that are even higher ($0.113 \text{ e} \cdot \text{\AA}^{-3}$) which means that there is *a priori* no reason why a $\text{Sr}_6\text{F}_9^{3+}$ core could not be formed.

Complex $\text{Sr}_6\text{N}''_4\text{F}_8 \cdot (\text{Me}_6\text{Tren})_2$ displays poor solubility but dissolved in a mixture of C_6D_6 and $\text{C}_6\text{D}_5\text{Br}$ ($1:1$) ^1H NMR and ^{19}F

NMR spectra could be obtained (Figures S26–27). Observation of only one sharp ^{19}F signal implies a higher symmetry than in the crystal structure in which two different types of F atoms are present (Figure S27). The higher symmetry in solution is likely due to dynamic coordination of the Me_6Tren ligand giving rise to an average structure with four equal equatorial $\text{Sr}-\text{N}''$ units and two equal axial $\text{Sr} \cdots \text{Me}_6\text{Tren}$ units. The complex is stable in solution and can even be recrystallized from the benzene/bromobenzene mixture. Its rather poor solubility precludes the recording of a $^{13}\text{C}\{^1\text{H}\}$ spectrum but the ^{13}C chemical shifts could be obtained by HSQC (Figure S29). Improved solubility of $\text{Sr}_6\text{N}''_4\text{F}_8 \cdot (\text{Me}_6\text{Tren})_2$ was obtained upon heating in a mixture of C_6D_6 and a small quantity of THF-*d*₈, however, rapid complex degradation was observed, indicated by numerous new ^{19}F NMR signals. The isolation of a colorless crystal from this solution shed some light on the decomposition process.

A larger neutral aggregate of formula $\text{Sr}_{16}\text{N}''_8\text{F}_{24} \cdot (\text{THF})_{12}$ crystallized as a centrosymmetric entity in which all tetradentate Me_6Tren ligands have been replaced by THF ligands (Figure 3a). This large aggregate can be seen as four fused Sr_6 -octahedra (Figure 3b) and, similar to the smaller Sr fluoride cluster $\text{Sr}_6\text{N}''_4\text{F}_8 \cdot (\text{Me}_6\text{Tren})_2$, it can be regarded as a sub-unit of the SrF_2 fluorite crystal lattice. The large $\text{Sr}_{16}\text{F}_{24}^{8+}$ core is protected for further growth by eight shielding N'' anions and twelve THF ligands. The $\text{Sr} \cdots \text{Sr}$ distances in the Sr_{16} -cluster (avg. 3.9863 Å) are slightly larger than in the Sr_6 -cluster (avg. 3.9343 Å). The Sr_6 - and Sr_{16} -cluster show equal average $\text{Sr}-(\mu_3\text{-F})$ bond distances of ≈ 2.433 Å but the average $\text{Sr}-(\mu_4\text{-F})$ bond distance in the Sr_{16} -cluster is somewhat larger: 2.499 Å (Table S2).

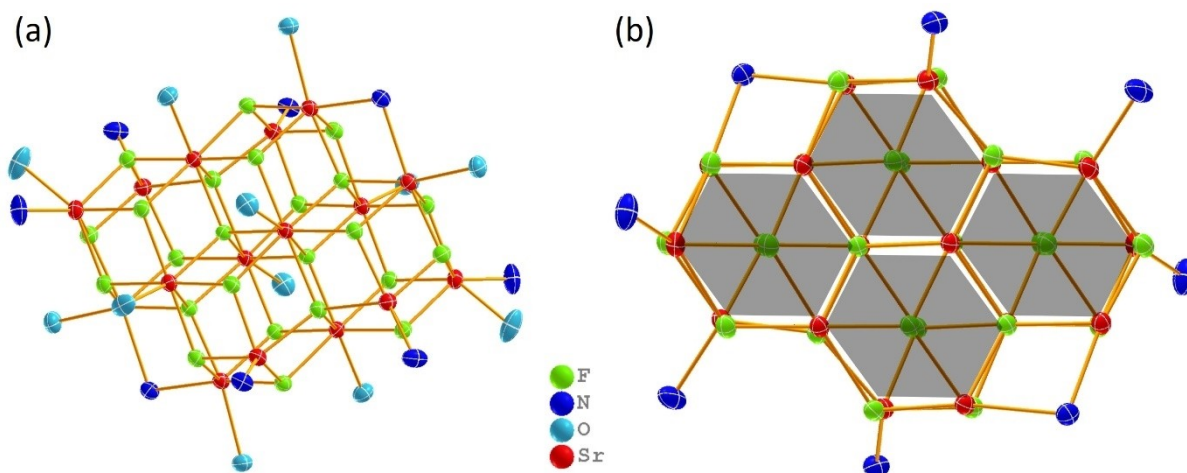


Figure 3. (a) The crystal structure of $\text{Sr}_{16}\text{N}_8\text{F}_{24} \cdot (\text{THF})_{12}$ (Me_3Si units and CH_2 fragments have been omitted for clarity). (b) The $\text{Sr}_{16}\text{F}_{24}^{8+}$ core described as four fused Sr_6 -octahedra. All ellipsoids are shown with 50% probability.

Proposed mechanism for hydrodehalogenation of aromatic halobenzenes

While the hydrodehalogenation of alkyl halogenides with metal hydride reagents follows standard nucleophilic substitution or elimination routes, there has been some discussion on the hydrodehalogenation of halobenzenes. For the hydrodehalogenation of $\text{C}_6\text{H}_5\text{X}$ with KH , Pierre observed a reactivity order: $\text{X} = \text{Cl} < \text{Br} < \text{I}$.^[26] For an $\text{S}_{\text{N}}\text{Ar}$ mechanism via a Meisenheimer anion the opposite order would be expected: $\text{I} < \text{Br} < \text{Cl} < \text{F}$. The fast reaction for fluorobenzene may seem counterintuitive due to the strong C–F bond, however, cleavage of the strong C–F bond is in this case not rate-determining. The rate-determining step in this two-step reaction is formation of the Meisenheimer anion, an intermediate in which ring aromaticity is lost (Figure 4a) and which is stabilized by electronegative substituents like F. The barrier for the second step in which C–F bond cleavage takes place is much lower due to rearomatization. In order to explain the observed reactivity order, Pierre proposed a one-step concerted nucleophilic aromatic substitution ($\text{cS}_{\text{N}}\text{Ar}$), a mechanism which is currently in focus of modern organic chemistry.^[57] The energy barrier for this reaction mechanism is determined by C–X bond strengths (Figure 4a). Calculations by Murphy and coworkers confirmed this mechanism for the hydrodeiodination of $\text{C}_6\text{H}_5\text{I}$ with KH .^[27] Also the Hill and Maron groups reported this mechanism for hydrodehalogenation ($\text{X} = \text{Cl}$ or Br) with a Ca hydride complex. We here report DFT mechanisms for the hydrodehalogenation of $\text{C}_6\text{H}_5\text{X}$ ($\text{X} = \text{Br}$ or I) with Sr hydride reagents (B3PW91/def2tzvp//B3PW91/def2svp). The complete energy profile for reaction of monomeric ($^{\text{DIPeP}}\text{BDI}$)SrH with PhI can be found in the Supporting Information (Figure S64). This also contains the full profile for a dimeric model system [$(^{\text{Ph}}\text{BDI})\text{SrH}$]₂ in which for simplicity the DIPeP substituents in the ligand have been replaced by smaller Ph groups; Figure S65. For comparison with an earlier reported pathway, we calculated the hydrodebromination of $\text{C}_6\text{H}_5\text{Br}$ with the model system [$(^{\text{DIPeP}}\text{BDI})\text{SrH}$]₂ in which the DIPeP substituents

have been replaced by somewhat smaller DIPP groups (Figure 4b). The activation barrier for Br–H exchange is $\Delta H = 30.3 \text{ kcal} \cdot \text{mol}^{-1}$. Hill and Maron reported for the same reaction with [$(^{\text{DIPP}}\text{BDI})\text{CaH}$]₂ a slightly higher barrier of $\Delta H = 31.6 \text{ kcal} \cdot \text{mol}^{-1}$.^[32] Since these calculations were done at a different level (B3PW91/6-311+G*), we repeated these calculations using our level of theory and found a considerably higher barrier of $34.5 \text{ kcal} \cdot \text{mol}^{-1}$. This demonstrates that the barrier for the Sr hydride reagent is circa $4 \text{ kcal} \cdot \text{mol}^{-1}$ lower than for the comparable Ca hydride reagent, supporting the experimentally observed higher reactivity of Sr complexes. The transition states clearly show a concerted process with concomitant hydride attack and C–Br bond cleavage (Figure 4c). The transition state for the Sr hydride dimer is not only significantly lower in energy than that for the analogue Ca hydride complex but also slightly earlier in respect of bond breaking and bondmaking.

We therefore propose a $\text{cS}_{\text{N}}\text{Ar}$ mechanism but have indications for competing mechanisms. Especially for the heavier halobenzenes (Br and I), some gas development was observed during reaction with [$(^{\text{DIPeP}}\text{BDI})\text{SrH}$]₂. Traces of H_2 in the ^1H NMR confirmed this observation. This points to a competing mechanism in which *ortho*-deprotonation and concomitant H_2 production is followed by Ae–X elimination and benzyne formation. Traces of biphenyl and terphenyl, detected by GC-MS analysis, support that this mechanism could play a minor role. We note that this may also be the case in hydrodehalogenation with [$(^{\text{DIPP}}\text{BDI})\text{CaH}$]₂ for which Wilson and Hill likewise report effervescence.^[58] A strong argument in favor of a $\text{cS}_{\text{N}}\text{Ar}$ mechanism (and precluding a benzyne mechanism) is the observation that 2,6-dimethyl-fluorobenzene, in which the *ortho*-positions are protected, could also be converted to *meta*-xylene (Table 1, entries 7–9). At this stage, however, we also do not rule out contributions of a SET mechanism as observed by Murphy.^[27]

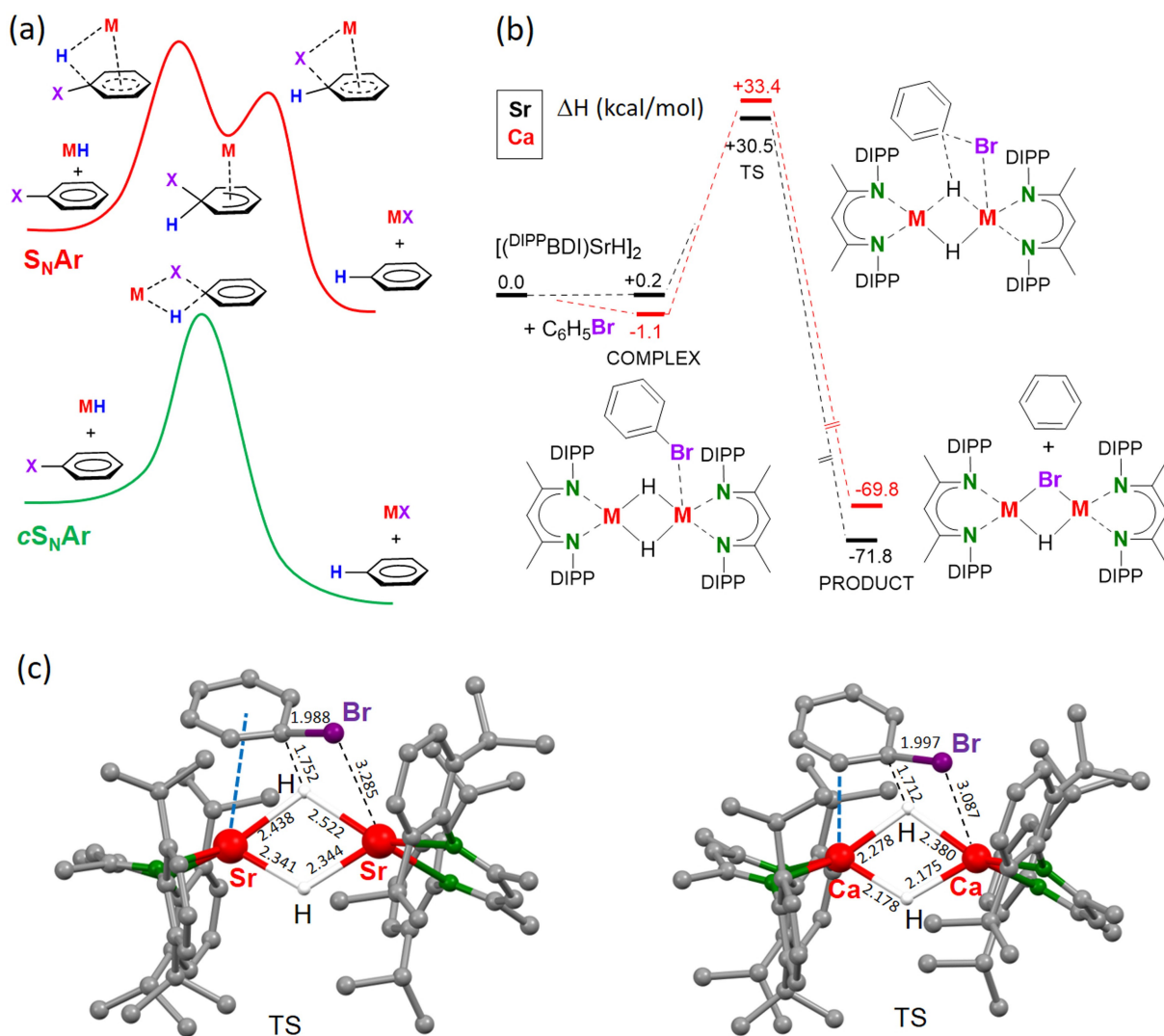


Figure 4. (a) Reaction of metal hydride (MH) with halobenzene (C₆H₅X) via a *S_NAr* or *cS_NAr* mechanism. (b) Energy profile (ΔH in kcal/mol) for the hydrodehalogenation of C₆H₅Br with [(DIPePBDI)SrH]₂ (black) or [(DIPePBDI)CaH]₂ (red); B3PW91/def2tvp//B3PW91/def2svp. (c) Calculated transition states for the hydrodehalogenation of C₆H₅Br with [(DIPePBDI)SrH]₂ (left) or [(DIPePBDI)CaH]₂ (right).

Conclusion

Hydrodehalogenation of aromatic halides with [(DIPePBDI)SrH]₂ gave after crystallization from THF well defined dimers [(DIPePBDI)SrX]·THF₂ (X = F, Cl, Br, I). These could not be regenerated back to the Sr hydride starting material by reaction with silanes which precludes a catalytic protocol. The bulky DIPePBDI ligand, which is needed to stabilize the Sr hydride complex, hinders the hydrodehalogenation reaction and therefore more open Ae metal hydride systems have been tested. Mixtures of AeN''₂ and PhSiH₃ gave less defined but more robust Ae metal hydride clusters of formula Ae_xN''_yH_z (y + z = 2x) which in solution are also stable at the higher temperature of 120 °C. The conversion rate increases with increasing metal size (Ca < Sr < Ba) and increasing halogen size (F < Cl < Br < I). At this temperature, the BaN''₂/PhSiH₃ combination was found to be especially effective for the hydrodefluorination of difficult substrates like C₆H₅F and

even 2,6-dimethyl-fluorobenzene, an electron-rich substrate with methylated *ortho*-positions which could be converted to *m*-xylene. Although the *in situ* generated Ae metal hydride reagents are not as defined as [(DIPePBDI)SrH]₂, it was possible to isolate and structurally characterize distinct Sr fluoride clusters. Hydrodefluorination of primary, secondary and tertiary alkyl-fluorides was also achieved. In this case the following order of reactivity was found: Ca < Sr > Ba. This exceptional reactivity order can be explained by the poor solubility of the Ba amide-hydride clusters, corroborated by the precipitation of considerable quantities of an insoluble Ba species. These AeN''₂/PhSiH₃ combinations (Ae = Sr, Ba) could even fully convert SF₆ at room temperature to give undefined decomposition products.

In agreement with earlier work, hydride-halogenide exchange in aromatic substrates like C₆H₅X is proposed to proceed through direct nucleophilic aromatic substitution. The reactivity order for hydrodehalogenation of C₆H₅X (F < Cl < Br < I) rules

out a two-step nucleophilic aromatic substitution mechanism with a Meisenheimer intermediate. Instead, a concerted mechanism is proposed ($\text{C}_{\text{S}}\text{N}_{\text{Ar}}$). DFT calculations on the hydrodeiodination of $\text{C}_6\text{H}_5\text{I}$ with a dimeric β -diketiminate Sr hydride complex support this conclusion, however, smaller contributions from benzyne or radical formation as alternative mechanisms cannot be fully ruled out.

The most important conclusion of this work is that either defined or undefined Ae metal hydride clusters are highly effective in the hydrodehalogenation of aromatic halobenzenes or alkylfluorides. Their reactivity increases with metal size ($\text{Ca} < \text{Sr} < \text{Ba}$) but the larger Ba reagents may suffer from solubility problems. Especially for the most reactive Sr and Ba hydride complexes, we continue to explore further applications.

Experimental Section

General Experimental Procedures

All experiments were conducted in dry glassware under an inert nitrogen atmosphere by applying standard Schlenk techniques or gloveboxes (MBraun) using freshly dried and degassed solvents. Benzene, toluene, pentane and hexane were degassed with nitrogen, dried over activated aluminum oxide (Innovative Technology, Pure Solv 400-4-MD, Solvent Purification System) and then stored under inert atmosphere. THF was dried over molecular sieves (3 Å) and distilled from sodium afterwards. Deuterated benzene (C_6D_6 , 99.6+ %D) and toluene- d_8 (99.6+ %D) were purchased from Deutero GmbH and Euriso-top, degassed and dried over molecular sieves (3 Å). Following reagents were obtained commercially and used without further purification: PhSiH_3 (Alfa Aesar, 97%), 1-fluoradamantane (TCI) and SF_6 (3.0, Westfalen). Fluorohexane (abcr, 99%), fluorocyclohexane (Acros Organics, 97%), 2-fluoro-m-xylene (Alfa Aesar, 98%), iodobenzene (PhI, Alfa Aesar 98%), bromobenzene (PhBr, Sigma Aldrich, 99%), chlorobenzene (PhCl, Alfa Aesar, 99%), fluorobenzene (PhF, Fluorochem, 98%) and 1,2-difluorobenzene (PhF₂, Fluorochem, 98%) were distilled from CaH_2 and stored over molecular sieves (3 Å). The following compounds were synthesized according to literature procedures: $[(^{\text{DIPeP}}\text{BDI})\text{SrH}]_2$, $[\text{Ca}(\text{N}(\text{SiMe}_3)_2)_2 (\text{CaN}''_2)]$, $[\text{Sr}(\text{N}(\text{SiMe}_3)_2)_2 (\text{SrN}''_2)]$ and $[\text{Ba}(\text{N}(\text{SiMe}_3)_2)_2 (\text{BaN}''_2)]$.^[59] NMR spectra were measured on Bruker Avance III HD 400 MHz and Bruker Avance III HD 600 MHz spectrometers. Chemical shifts (δ) are denoted in ppm (parts per million), coupling constants in Hz (Hertz). For describing signal multiplicities common abbreviations are used: s (singlet), d (doublet), t (triplet), q (quartet), quin (quintet), m (multiplet) and br (broad). Spectra were referenced to the solvent residual signal. Elemental analysis was performed with an Hekatech Eurovector EA3000 analyzer. GC-MS measurements were performed on a Thermo Scientific™ Trace™ 1310 gas chromatography system (carrier gas Helium) with detection by a Thermo Scientific™ ISQ™ LT Single Quadrupole mass spectrometer. A Phenomenex® Zebron™ ZB-5 GC column of the dimensions 0.25 mm×30 m with a film thickness of 0.25 μm was used. The samples (1 μL) were injected with an Instant Connect-SSL Module in the split mode (injector temperature: 280 °C). Temperature programs were started at 40 °C followed by heating ramps, optimized for the separation problem, until 280 °C. Baseline separation of each analyte was achieved by choosing the different temperature programs. The molecular identities were confirmed by comparison with entries in the NIST/EPA/NIH mass spectral library (v2.2, built June 10 2014). All crystal structures have been measured on a SuperNova (Agilent) diffractometer with dual Cu and Mo microfocus sources and an Atlas S2 detector.

Synthesis of $[(^{\text{DIPeP}}\text{BDI})\text{SrI} \cdot \text{THF}]_2$: In a J-Young NMR tube $[(^{\text{DIPeP}}\text{BDI})\text{SrH}]_2$ (102.6 mg, 165.9 μmol) was dissolved in PhI (520 μL). The solution was stirred at ambient temperature for 1 h and the solvent removed subsequently *in vacuo*. The oily residue was dissolved in a mixture of hexane (400 μL) and THF (30 μL), filtered and stored at room temperature overnight, affording colorless crystals suitable for X-ray diffraction analysis. The supernatant was decanted, the product washed with cold pentane (−20 °C, 2×0.5 ml) and dried under high vacuum. $[(^{\text{DIPeP}}\text{BDI})\text{SrI} \cdot \text{THF}]_2$ was obtained as colorless crystalline blocks (58.2 mg, 71.3 μmol , 43%). ^1H NMR (600.13 MHz, C_6D_6 , 298 K): δ = 0.90 (t, 3J = 7.4 Hz, 12H, CH_3), 1.01 (t, 3J = 7.4 Hz, 12H, CH_3), 1.29–1.31 (m, 4H, OCH_2CH_2), 1.65–1.72 (m, 8H, CH_2), 1.70 (s, 6H, CH_3 -backbone), 1.71–1.76 (m, 4H, CH_2), 1.82–1.89 (m, 4H, CH_2), 2.91 (quint, 3J = 6.3 Hz, 4H, CH), 3.66–3.68 (m, 4H, OCH_2CH_2), 4.83 (s, 1H, CH-backbone), 7.10–7.14 (m, 6H, CH-arom), 12.3 (CH₃-backbone), 25.4 (OCH_2CH_2), 26.4 (CH_2), 28.1 (CH_2), 41.2 (CH), 69.2 (OCH_2CH_2), 93.0 (CH-backbone), 123.3 (C-arom), 125.8 (C-arom), 138.2 (C-arom), 149.1 (C-arom), 165.0 (CN-backbone) ppm. Elemental analysis calculated for $\text{C}_{82}\text{H}_{130}\text{I}_2\text{Sr}_2\text{N}_4\text{O}_2$ (M = 1633.02 g/mol): C 60.31, H 8.02, N 3.43; Found: C 60.16, H 8.06, N 3.46.

Synthesis of $[(^{\text{DIPeP}}\text{BDI})\text{SrBr} \cdot \text{THF}]_2$: In a J-Young NMR tube $[(^{\text{DIPeP}}\text{BDI})\text{SrH}]_2$ (92.2 mg, 149.1 μmol) was dissolved in PhBr (520 μL , gas evolution observed) and the solution was stirred at ambient temperature overnight (14 h). Subsequently the solvent was removed and the oily residue dried under high vacuum. Crystals of $[(^{\text{DIPeP}}\text{BDI})\text{SrBr} \cdot \text{THF}]_2$ suitable for X-ray diffraction analysis were obtained by slow diffusion of THF to a diluted hexane solution (500 μL) at ambient temperature overnight (18 h). The crystals were isolated by decantation, washed with cold pentane (−20 °C, 2×0.5 ml) and dried under high vacuum. $[(^{\text{DIPeP}}\text{BDI})\text{SrBr} \cdot \text{THF}]_2$ was obtained as pale orange colored small crystalline blocks (82.6 mg, 107.3 μmol , 72%). ^1H NMR (600.13 MHz, C_6D_6 , 298 K): δ = 0.89 (t, 3J = 7.4 Hz, 12H, CH_3), 0.97 (t, 3J = 7.3 Hz, 12H, CH_3), 1.36–1.38 (m, 4H, OCH_2CH_2), 1.62–1.64 (m, 6H, CH_2), 1.68 (s, 6H, CH_3 -backbone), 1.69–1.77 (m, 10H, CH_2), 2.86 (quint, 3J = 6.3 Hz, 4H, CH), 3.69–3.71 (m, 4H, OCH_2CH_2), 4.76 (s, 1H, CH-backbone), 7.08–7.13 (m, 6H, CH-arom) ppm. ^{13}C NMR (150.92 MHz, C_6D_6 , 298 K): δ = 11.5 (CH_3), 12.2 (CH_3), 25.2 (CH_3 -backbone), 25.5 (OCH_2CH_2), 26.4 (CH_2), 27.9 (CH_2), 41.2 (CH), 69.0 (OCH_2CH_2), 93.2 (CH-backbone), 123.2 (C-arom), 125.7 (C-arom), 138.7 (C-arom), 148.9 (C-arom), 164.9 (CN-backbone) ppm. Elemental analysis calculated for $\text{C}_{82}\text{H}_{130}\text{Br}_2\text{Sr}_2\text{N}_4\text{O}_2$ (M = 1539.02 g/mol): C 64.00, H 8.51, N 3.64; Found: C 63.96, H 8.71, N 3.63.

Synthesis of $[(^{\text{DIPeP}}\text{BDI})\text{SrCl} \cdot \text{THF}]_2$:

In a J-Young NMR tube $[(^{\text{DIPeP}}\text{BDI})\text{SrH}]_2$ (104.4 mg, 168.8 μmol) was dissolved in PhCl (520 μL). The solution was heated to 60 °C and stirred at this temperature for 20 h. The solvent was pumped off and the sticky semi solid dried under high vacuum. The residue was dissolved in hexane (300 μL), filtered and covered with a mixture of hexane (200 μL) and THF (30 μL). Leaving it standing overnight at room temperature gave yellowish crystalline blocks of $[(^{\text{DIPeP}}\text{BDI})\text{SrCl} \cdot \text{THF}]_2$ suitable for X-ray diffraction analysis. The supernatant was decanted, the crystals washed with cold pentane (−20 °C, 2×0.5 ml) and dried under high vacuum (64.9 mg, 89.5 μmol , 53%). ^1H NMR (600.13 MHz, C_6D_6 , 298 K): δ = 0.89 (t, 3J = 7.4 Hz, 12H, CH_3), 0.92 (t, 3J = 7.3 Hz, 12H, CH_3), 1.40–1.43 (m, 4H, OCH_2CH_2), 1.62–1.64 (m, 6H, CH_2), 1.64–1.70 (m, 10H, CH_2), 1.68 (s, 6H, CH_3 -backbone), 2.83 (quint, 3J = 6.4 Hz, 4H, CH), 3.67–3.69 (m, 4H, OCH_2CH_2), 4.74 (s, 1H, CH-backbone), 7.07–7.12 (m, 6H, CH-arom) ppm. ^{13}C NMR (150.92 MHz, C_6D_6 , 298 K): δ = 11.6 (CH_3), 12.1 (CH_3), 25.1 (CH_3 -backbone), 25.6 (OCH_2CH_2), 26.6 (CH_2), 27.9 (CH_2), 41.3 (CH), 68.8 (OCH_2CH_2), 93.3 (CH-backbone), 123.1 (C-arom), 125.6 (C-arom), 138.9 (C-arom), 148.8 (C-arom), 164.7 (CN-backbone) ppm. Elemental

tal analysis calculated for $\text{C}_{82}\text{H}_{130}\text{Cl}_2\text{Sr}_2\text{N}_4\text{O}_2$ ($M = 1450.11$ g/mol): C 67.92, H 9.04, N 3.86; Found: C 68.09, H 9.34, N 3.65.

Synthesis of $[(^{\text{DIPeP}}\text{BDI})\text{SrF} \cdot \text{THF}]_2$: In a J-Young NMR tube $[(^{\text{DIPeP}}\text{BDI})\text{SrH}]_2$ (95.7 mg, 154.7 μmol) was dissolved in PhF_2 (520 μL). The solution was stirred at 60 °C for 4 h and the solvent subsequently removed *in vacuo*. The powdery residue was dissolved in hexane (400 μL), filtered and THF (30 μL , diluted with hexane (100 μL) was added slowly. Small, pale yellow, crystals of $[(^{\text{DIPeP}}\text{BDI})\text{SrF} \cdot \text{THF}]_2$ suitable for X-ray diffraction analysis formed overnight at ambient temperature. The supernatant was decanted, the crystals washed with cold pentane (−20 °C, 2 × 0.5 ml) and dried under high vacuum (61.4 mg, 86.6 μmol , 56%). ^1H NMR (600.13 MHz, C_6D_6 , 298 K): $\delta = 0.73$ (t, $^3J = 7.3$ Hz, 12H, CH_3), 0.90 (t, $^3J = 7.4$ Hz, 12H, CH_3), 1.43–1.45 (m, 4H, OCH_2CH_2), 1.49–1.55 (m, 4H, CH_2), 1.55–1.61 (m, 4H, CH_2), 1.61–1.66 (m, 8H, CH_2), 1.69 (s, 6H, CH_3 -backbone), 2.78 (quint, $^3J = 6.7$ Hz, 4H, CH), 3.66–3.69 (m, 4H, OCH_2CH_2), 4.73 (s, 1H, CH-backbone), 7.03–7.05 (m, 4H, CH-arom), 7.08–7.11 (m, 2H, CH-arom) ppm. ^{13}C NMR (150.92 MHz, C_6D_6 , 298 K): $\delta = 12.2$ (CH_3), 12.3 (CH_3), 24.9 (CH_3 -backbone), 25.3 (OCH_2CH_2), 27.8 (CH_2), 28.3 (CH_2), 41.7 (CH), 68.3 (OCH_2CH_2), 93.1 (CH-backbone), 123.2 (C-arom), 125.1 (C-arom), 139.1 (C-arom), 149.3 (C-arom), 164.0 (CN-backbone) ppm. ^{19}F NMR (564.63 MHz, C_6D_6 , 298 K): $\delta = -51.5$ (Sr-F) ppm. Elemental analysis Calculated for $\text{C}_{82}\text{H}_{130}\text{F}_2\text{Sr}_2\text{N}_4\text{O}_2$ ($M = 1417.20$ g/mol): C 69.50, H 9.25, N 3.95; Found: C 69.41, H 9.37, N 3.88.

Synthesis of $[\text{Sr}_6\text{N}''_4\text{H}_9 \cdot (\text{Me}_6\text{Tren})_3]^+[\text{SrN}''_3]^-$: SrN''_2 (100 mg, 0.245 mmol, 2.33 eq) and Me_6Tren (28.1 μL , 24.1 mg, 0.105 mmol, 1 eq) were suspended in 3 mL of benzene. PhSiH_3 (38.8 μL , 34.1 mg, 0.315 mmol, 3 eq) was added to the stirring mixture. The suspension was stirred until all solid material dissolved and the formation of a two-phase system (brown oil and colorless solution) was observed. A colorless crystal was isolated from the reaction mixture after resting at room temperature for 27 days and identified by X-ray diffraction as $[\text{Sr}_6\text{N}''_4\text{H}_9 \cdot (\text{Me}_6\text{Tren})_3]^+[\text{SrN}''_3]^-$. Larger quantities could not be obtained.

Synthesis of $\text{Sr}_6\text{N}''_4\text{F}_8 \cdot (\text{Me}_6\text{Tren})_2$: To a stirred solution of SrN''_2 (500 mg, 1.22 mmol, 2.33 eq) in toluene (5 mL) was added in sequence: fluorobenzene (833 μL), 1-fluorohexane (333 μL , 267 mg, 2.56 mmol, 2.1 eq) and Me_6Tren (333 μL , 287 mg, 1.24 mmol, 1.02 eq). Phenylsilane (227 μL , 199 mg, 1.84 mmol, 1.5 eq.) was added slowly to the stirring reaction mixture and the resulting dark orange solution was stirred at 80 °C for 2.5 h. All volatiles were removed under reduced pressure, and the brown oily residue was dried *in vacuo* at room temperature. The oil was washed with pentane (3 × 4 mL, sonification) to obtain a brownish powder. All liquids were removed under reduced pressure and the residue recrystallized from a toluene (1 mL), fluorobenzene (1 mL) mixture to obtain clear, colorless crystals overnight. The crystals (36 mg, 0.020 mmol, 9.9% based on SrN''_2) were washed with toluene (1.5 mL) and pentane (3 × 2 mL) and dried at room temperature in a glovebox under N_2 -atmosphere. The solid material was dried under vacuum to remove crystal solvent prior to NMR investigations. Yield was calculated on the basis that six eq of SrN''_2 are needed to form one eq of $\text{Sr}_6\text{N}''_4\text{F}_8 \cdot (\text{Me}_6\text{Tren})_2$. ^1H NMR (600.13 MHz, $\text{C}_6\text{D}_6/\text{BrC}_6\text{D}_5$ ratio 1:1, 298 K): $\delta = 2.63$ (t, $^3J = 6.8$, 4H, CH_2), 2.37 (d, $J = 7.0$, 4H, CH_2), 2.15 (s, 24H, $\text{N}(\text{CH}_3)_2$), 2.12 (s, 12H, $\text{N}(\text{CH}_3)_2$), 2.03–1.97 (m, 8H, CH_2), 0.30 (s, 72H, $\text{Si}(\text{CH}_3)_3$) ppm. ^{19}F NMR (564.63 MHz, $\text{C}_6\text{D}_6/\text{BrC}_6\text{D}_5$ ratio 1:1, 298 K): $\delta = -70.47$ ppm. Poor solubility did not allow for $^{13}\text{C}\{^1\text{H}\}$ NMR analysis. HSQC (Heteronuclear Single Quantum Coherence) ^1H - ^{13}C NMR ((600.13, 150.92) MHz, C_6D_6): $\delta = (2.63/53.96, \text{CH}_2)$, (2.37/58.49, CH_2), (2.15/45.39, $\text{N}(\text{CH}_3)_2$), (2.11/51.29, $\text{N}(\text{CH}_3)_2$), (2.00/56.20, CH_2), (0.31/7.55, $\text{Si}(\text{CH}_3)_3$) ppm. Elemental analysis calculated for $\text{C}_{55}\text{H}_{140}\text{F}_8\text{N}_{12}\text{Si}_6\text{Sr}_6$ ($M = 1872.20$ g/mol): C: 35.29; H: 7.54; N: 8.98. Found: C 35.12, H 7.39, N 8.68.

Synthesis of $\text{Sr}_{16}\text{N}''_8\text{F}_{24} \cdot (\text{THF})_{12}$: In a J-Young NMR tube, $\text{Sr}_6\text{N}''_4\text{F}_8 \cdot (\text{Me}_6\text{Tren})_2$ (20 mg) was suspended in 500 μL C_6D_6 followed by 50 μL THF- d_8 . The suspension was quickly heated to 60 °C to obtain a clear solution. The solution was filtered and few, very small crystals suitable for single crystal X-ray diffraction were observed after one week at room temperature. Larger quantities could not be obtained.

Hydrodefluorination with $\text{AeN}''_2/\text{PhSiH}_3$ (Ae = Ca, Sr, Ba): A J-Young NMR tube was charged with AeN''_2 (Ca: 16 mg, 0.044 mmol; Sr: 20 mg, 0.049 mmol, Ba: 20 mg, 0.044 mmol), followed by addition of toluene- d_8 (550 μL) and two equivalent of the organofluorine compound. Phenylsilane (3 or 10 eq.) was added to the solution. In case BaN''_2 was used, this was followed by rapid formation of precipitate. The mixture was heated to 120 °C (for 6 or 12 h) or to 60 °C (for 24 h). The product mixture was quenched with diethylether (500 μL) and distilled water (20 μL), filtered and analyzed by GC/MS and/or NMR.

Preparation of a SF_6 solution in toluene: Degassed toluene (10 mL) was placed in a 50 mL round-bottom Schlenk flask. Rapidly stirring the solution, a gentle vacuum was applied which led to cooling. The cold solution was saturated with SF_6 gas and stirred under SF_6 atmosphere (1.06 bar) for one hour. The solution was subsequently exposed a second time to 1.06 bar of SF_6 pressure. The presence of SF_6 was checked prior to each reaction by ^{19}F NMR. ^{19}F NMR (564.63 MHz, $\text{C}_7\text{H}_8/\text{C}_6\text{D}_6$, 298 K): $\delta = -58.3$ (S-F) ppm.

Reactions of $\text{AeN}''_2/\text{PhSiH}_3$ (Ae = Sr, Ba) with SF_6 : A J-Young NMR tube was charged with AeN''_2 (Sr: 20 mg, 0.049 mmol; Ba: 20 mg, 0.044 mmol), followed by the saturated SF_6 solution in toluene (300 μL) and benzene- d_6 (550 μL). Four equivalents of phenylsilane (Sr: 24.2 μL , 0.196 mmol; Ba: 21.7 μL , 0.176 mmol) were added to the solution. This was in both cases followed by immediate formation of a yellowish precipitate. This suspension was stirred for 12 h at room temperature, during which time additional precipitate was formed. The supernatant was decanted and the yellow powder dried *in vacuo* and characterized by elemental analysis. In reaction with $\text{BaN}''_2/\text{PhSiH}_3$ following values were found: C 24.14%, H 3.77%, N 1.64%, S 1.77%.

Deposition Numbers 2091324 (for $[(^{\text{DIPeP}}\text{BDI})\text{Sr}(\text{THF})]_2$), 2091325 (for $[(^{\text{DIPeP}}\text{BDI})\text{SrBr}(\text{thf})]_2$), 2091326 (for $[(^{\text{DIPeP}}\text{BDI})\text{SrCl}(\text{thf})]_2$), 2091327 (for $[(^{\text{DIPeP}}\text{BDI})\text{SrF}(\text{thf})]_2$), 2091328 (for $[\text{Sr}_6\text{N}''_4\text{H}_9 \cdot (\text{Me}_6\text{Tren})_3]^+[\text{SrN}''_3]^-$), 2091329 (for $\text{Sr}_6\text{N}''_4\text{F}_8 \cdot (\text{Me}_6\text{Tren})_2$), and 2091330 (for $\text{Sr}_{16}\text{N}''_8\text{F}_{24} \cdot (\text{THF})_{12}$) contain the supplementary crystallographic data for this paper. These data are provided free of charge by the joint Cambridge Crystallographic Data Centre and Fachinformationszentrum Karlsruhe Access Structures service www.ccdc.cam.ac.uk/structures.

Supporting Information

(See footnote on the first page of this article): ^1H , ^{29}Si , ^{19}F , ^{13}C NMR spectra, crystallographic details including ORTEP plots, details for the DFT calculations including XYZ-files.

The authors declare no competing financial interest.

Acknowledgements

We acknowledge C. Wronna and A. Roth for CHN analyses and Dr. C. Färber and J. Schmidt for assistance with NMR analyses. We thank the Deutsche Forschungsgemeinschaft for funding (HA

3218/9-1). Open Access funding enabled and organized by Projekt DEAL.

Conflict of Interest

The authors declare no conflict of interest.

Keywords: Alkaline-earth metal • DFT calculation • Hydride • Hydrodehalogenation

- [1] H. Amii, K. Uneyama, *Chem. Rev.* **2009**, *109*, 2119–2183.
- [2] F. J. Urbano, J. M. Marinas, *J. Mol. Catal. A* **2001**, *173*, 329–345.
- [3] Z. Ainsbinder, L. E. Manzer, M. J. Nappa, in *Environ. Catal.*, Wiley, **1999**, pp. 197–212.
- [4] M. Hudlicky, *J. Fluorine Chem.* **1989**, *44*, 345–359.
- [5] D. Schrenk, M. Bignami, L. Bodin, J. K. Chipman, J. del Mazo, B. Grasl-Kraupp, C. Hogstrand, L. Hoogenboom, J. C. Leblanc, C. S. Nebbia, E. Ntzani, A. Petersen, S. Sand, T. Schwerdtle, C. Vleminckx, H. Wallace, B. Bruschweiler, P. Leonards, M. Rose, M. Binaglia, Z. Horváth, L. Ramos Bordajandi, E. Nielsen, *EFSA J.* **2020**, *18*, 1–220.
- [6] S. J. Blanksby, G. B. Ellison, *Acc. Chem. Res.* **2003**, *36*, 255–263.
- [7] Q. Shen, Y. G. Huang, C. Liu, J. C. Xiao, Q. Y. Chen, Y. Guo, *J. Fluorine Chem.* **2015**, *179*, 14–22.
- [8] C. Bakewell, A. J. P. White, M. R. Crimmin, *Angew. Chem. Int. Ed.* **2018**, *57*, 6638–6642; *Angew. Chem.* **2018**, *130*, 6748–6752.
- [9] M. R. Crimmin, M. J. Butler, A. J. P. White, *Chem. Commun.* **2015**, *51*, 15994–15996.
- [10] T. Chu, Y. Boyko, I. Korobkov, G. I. Nikonov, *Organometallics* **2015**, *34*, 5363–5365.
- [11] C. Bakewell, A. J. P. White, M. R. Crimmin, *J. Am. Chem. Soc.* **2016**, *138*, 12763–12766.
- [12] C. Bakewell, B. J. Ward, A. J. P. White, M. R. Crimmin, *Chem. Sci.* **2018**, *9*, 2348–2356.
- [13] G. Coates, B. J. Ward, C. Bakewell, A. J. P. White, M. R. Crimmin, *Chem. A Eur. J.* **2018**, *24*, 16282–16286.
- [14] T. X. Gentner, B. Rösch, G. Ballmann, J. Langer, H. Elsen, S. Harder, *Angew. Chem. Int. Ed.* **2019**, *58*, 607–611; *Angew. Chem.* **2019**, *131*, 617–621.
- [15] B. Cui, S. Jia, E. Tokunaga, N. Shibata, *Nat. Commun.* **2018**, *9*, 1–8.
- [16] M. Batuecas, N. Gorgas, M. R. Crimmin, *Chem. Sci.* **2021**, *12*, 1993–2000.
- [17] W. Chen, T. N. Hooper, J. Ng, A. J. P. White, M. R. Crimmin, *Angew. Chem. Int. Ed.* **2017**, *56*, 12687–12691; *Angew. Chem.* **2017**, *129*, 12861–12865.
- [18] F. Rekhroukh, W. Chen, R. K. Brown, A. J. P. White, M. R. Crimmin, *Chem. Sci.* **2020**, *11*, 7842–7849.
- [19] I. Fujii, K. Semba, Q. Z. Li, S. Sakaki, Y. Nakao, *J. Am. Chem. Soc.* **2020**, *142*, 11647–11652.
- [20] D. D. L. Jones, I. Douair, L. Maron, C. Jones, *Angew. Chem. Int. Ed.* **2021**, *60*, 7087–7092.
- [21] A. Friedrich, J. Eyselein, J. Langer, C. Färber, S. Harder, *Angew. Chem. Int. Ed.* **2021**, anie.202103250.
- [22] H. Li, S. Liao, Y. Xu, *Chem. Lett.* **1996**, *25*, 1059–1060.
- [23] K. Fuchibe, T. Akiyama, *Synlett* **2004**, 1282–1284.
- [24] Y. Zhang, S. Liao, Y. Xu, D. Yu, Q. Shen, *Synth. Commun.* **1997**, *27*, 4327–4334.
- [25] K. Kikushima, M. Grellier, M. Ohashi, S. Ogoshi, *Angew. Chem. Int. Ed.* **2017**, *56*, 16191–16196; *Angew. Chem.* **2017**, *129*, 16409–16414.
- [26] H. Handel, M. A. Pasquini, J. L. Pierre, *Tetrahedron* **1980**, *36*, 3205–3208.
- [27] J. P. Barham, S. E. Dalton, M. Allison, G. Nocera, A. Young, M. P. John, T. McGuire, S. Campos, T. Tuttle, J. A. Murphy, *J. Am. Chem. Soc.* **2018**, *140*, 11510–11518.
- [28] S. Loisel, M. Branca, G. Mulas, G. Cocco, *Environ. Sci. Technol.* **1997**, *31*, 261–265.
- [29] S. Harder, J. Brettar, *Angew. Chem. Int. Ed.* **2006**, *45*, 3474–3478; *Angew. Chem.* **2006**, *118*, 3554–3558.
- [30] J. Spielmann, S. Harder, *Chem. A Eur. J.* **2007**, *13*, 8928–8938.
- [31] A. S. S. Wilson, M. S. Hill, M. F. Mahon, C. Dinoi, L. Maron, *Science* **2017**, *358*, 1168–1171.
- [32] A. S. S. Wilson, M. S. Hill, M. F. Mahon, C. Dinoi, L. Maron, *Tetrahedron* **2021**, 131931.
- [33] D. Schuhknecht, T. P. Spaniol, Y. Yang, L. Maron, J. Okuda, *Inorg. Chem.* **2020**, *59*, 9406–9415.
- [34] S. Brand, H. Elsen, J. Langer, S. Grams, S. Harder, *Angew. Chem. Int. Ed.* **2019**, *58*, 15496–15503; *Angew. Chem.* **2019**, *131*, 15642–15649.
- [35] B. Rösch, T. X. Gentner, H. Elsen, C. A. Fischer, J. Langer, M. Wiesinger, S. Harder, *Angew. Chem. Int. Ed.* **2019**, *58*, 5396–5401; *Angew. Chem.* **2019**, *131*, 5450–5455.
- [36] J. Martin, J. Eyselein, S. Grams, S. Harder, *ACS Catal.* **2020**, *10*, 7792–7799.
- [37] B. Maitland, M. Wiesinger, J. Langer, G. Ballmann, J. Pahl, H. Elsen, C. Färber, S. Harder, *Angew. Chem. Int. Ed.* **2017**, *56*, 11880.
- [38] M. Wiesinger, B. Maitland, C. Färber, G. Ballmann, C. Fischer, H. Elsen, S. Harder, *Angew. Chem. Int. Ed.* **2017**, *56*, 16654–16659; *Angew. Chem.* **2017**, *129*, 16881–16886.
- [39] J. Martin, C. Knüpfer, J. Eyselein, C. Färber, S. Grams, J. Langer, K. Thum, M. Wiesinger, S. Harder, *Angew. Chem. Int. Ed.* **2020**, *59*, 9102–9112; *Angew. Chem.* **2020**, *132*, 9187–9197.
- [40] A. Causero, G. Ballmann, J. Pahl, C. Färber, J. Intemann, S. Harder, *Dalton Trans.* **2017**, *46*, 1822–1831.
- [41] S. Nembenna, H. W. Roesky, S. Nagendran, A. Hofmeister, J. Magull, P. J. Wilbrandt, M. Hahn, *Angew. Chem. Int. Ed.* **2007**, *46*, 2512–2514; *Angew. Chem.* **2007**, *119*, 2564–2566.
- [42] T. X. Gentner, B. Rösch, K. Thum, J. Langer, G. Ballmann, J. Pahl, W. A. Donaubauer, F. Hampel, S. Harder, *Organometallics* **2019**, *38*, 2485–2493.
- [43] S. P. Sarish, H. W. Roesky, M. John, A. Ringe, J. Magull, *Chem. Commun.* **2009**, *3*, 2390.
- [44] S. Pillai Sarish, A. Jana, H. W. Roesky, T. Schulz, M. John, D. Stalke, *Inorg. Chem.* **2010**, *49*, 3816–3820.
- [45] H. Bauer, M. Alonso, C. Fischer, B. Rösch, H. Elsen, S. Harder, *Angew. Chem. Int. Ed.* **2018**, *57*, 15177–15182; *Angew. Chem.* **2018**, *130*, 15397–15402.
- [46] H. Bauer, M. Alonso, C. Färber, H. Elsen, J. Pahl, A. Causero, G. Ballmann, F. De Proft, S. Harder, *Nat. Catal.* **2018**, *1*, 40–47.
- [47] H. Bauer, K. Thum, M. Alonso, C. Fischer, S. Harder, *Angew. Chem. Int. Ed.* **2019**, *58*, 4248–4253; *Angew. Chem.* **2019**, *131*, 4292–4297.
- [48] H. Elsen, C. Fischer, C. Knüpfer, A. Escalona, S. Harder, *Chem. A Eur. J.* **2019**, *25*, 16141–16147.
- [49] M. Rigby, J. Mühle, B. R. Miller, R. G. Prinn, P. B. Krummel, L. P. Steele, P. J. Fraser, P. K. Salameh, C. M. Harth, R. F. Weiss, B. R. Grealley, S. O'Doherty, P. G. Simmonds, M. K. Vollmer, S. Reimann, J. Kim, K.-R. Kim, H. J. Wang, J. G. J. Olivier, E. J. Dlugokencky, G. S. Dutton, B. D. Hall, J. W. Elkins, *Atmos. Chem. Phys.* **2010**, *10*, 10305–10320.
- [50] D. K. Padma, A. R. Vasudeva Murthy, W. Becher, J. Massonne, *J. Fluorine Chem.* **1972**, *2*, 113–114.
- [51] M. Rueping, P. Nikolaienko, Y. Lebedev, A. Adams, *Green Chem.* **2017**, *19*, 2571–2575.
- [52] G. B. Deacon, P. C. Junk, G. J. Moxey, *Dalton Trans.* **2010**, *39*, 5620.
- [53] P. F. Lang, B. C. Smith, *Dalton Trans.* **2010**, *39*, 7786.
- [54] C. E. Messer, *J. Solid State Chem.* **1970**, *2*, 144–155.
- [55] R. D. Shannon, C. T. Prewitt, *Acta Crystallogr. Sect. B* **1969**, *25*, 925–946.
- [56] R. D. Shannon, *Acta Crystallogr. Sect. A* **1976**, *32*, 751–767.
- [57] E. E. Kwan, Y. Zeng, H. A. Besser, E. N. Jacobsen, *Nat. Chem.* **2018**, *10*, 917–923.
- [58] A. Wilson, *Frontiers of Organo- and Hydricalcium Chemistry*, University of Bath, **2018**.
- [59] M. Westerhausen, *Inorg. Chem.* **1991**, *30*, 96–101.

Manuscript received: June 22, 2021
Revised manuscript received: July 26, 2021
Accepted manuscript online: July 28, 2021